

Centre symmetric 3d effective actions for thermal $SU(N)$ Yang-Mills from strong coupling series

Jens Langelage,^a Stefano Lottini^b Owe Philipsen^b

^a*Fakultät für Physik, Universität Bielefeld,
Universitätsstr. 25, 33501 Bielefeld, Germany*

^b*Institut für Theoretische Physik, Goethe-Universität Frankfurt,
Max-von-Laue-Str. 1, 60438 Frankfurt am Main, Germany*

E-mail: jlang@physik.uni-bielefeld.de,
lottini@th.physik.uni-frankfurt.de,
philipsen@th.physik.uni-frankfurt.de

ABSTRACT: We derive three-dimensional, $Z(N)$ -symmetric effective actions in terms of Polyakov loops by means of strong coupling expansions, starting from thermal $SU(N)$ Yang-Mills theory in four dimensions on the lattice. An earlier action in the literature, corresponding to the (spatial) strong coupling limit, is thus extended by several higher orders, as well as by additional interaction terms. We provide analytic mappings between the couplings of the effective theory and the parameters N_τ, β of the original thermal lattice theory, which can be systematically improved. We then investigate the deconfinement transition for the cases $SU(2)$ and $SU(3)$ by means of Monte Carlo simulations of the effective theory. Our effective models correctly reproduce second order 3d Ising and first order phase transitions, respectively. Furthermore, we calculate the critical couplings $\beta_c(N_\tau)$ and find agreement with results from simulations of the 4d theory at the few percent level for $N_\tau = 4 - 16$.

KEYWORDS: Strong-coupling expansion, Lattice gauge theory, Effective theory, Deconfinement

ARXIV EPRINT: [1010.0951](https://arxiv.org/abs/1010.0951)

BI-TP-2010/32

Contents

1	Introduction	1
2	Derivation of the effective theory	2
2.1	General strategy and $SU(2)$	2
2.2	The spatial strong coupling limit	4
2.3	Leading order effective action	4
2.4	Higher order terms	6
2.5	The effective action for $SU(3)$	7
3	Numerical simulation of the effective theories	8
3.1	The one coupling model	8
3.2	A “sign problem” and its solution	9
3.3	Phase structure, critical coupling and finite size analysis	10
3.4	Critical coupling and order of the transition for $SU(3)$	11
3.5	Critical coupling and order of the transition for $SU(2)$	14
3.6	Two-coupling models for $SU(3)$	14
4	Mapping back to 4d Yang-Mills	16
5	Conclusions	18

1 Introduction

Non-abelian gauge theories at finite temperature are inherently non-perturbative, due to infrared problems for soft gauge fields [1]. The dynamical appearance of different scales, $\pi T, gT, g^2 T$ with gauge coupling g , has motivated effective theory methods, most notably dimensional reduction [2, 3]. The idea is to integrate over the hard scales perturbatively, whereupon a three-dimensional effective theory arises which is then easier to solve by non-perturbative means. A particularly successful application is the investigation of the electroweak phase transition as a function of the Higgs mass using the 3d effective theories [4, 5], which produced results at the few percent accuracy level compared to simulations of the full 4d theory [6].

In QCD, the same technique can be applied to observables in the deconfined phase only, because the reduction loses validity as the deconfinement transition is approached. An investigation of the phase diagram by similar methods would be particularly desirable, since lattice Monte Carlo studies at finite baryon density are beset by the sign-problem. Unfortunately, the QCD phase structure is not inherited by the dimensionally reduced model, which loses the $Z(N)$ symmetry of Yang-Mills theory in the perturbative reduction step

[7]. This has motivated alternative approaches, where the most general $Z(N)$ -symmetric theory is written down and the couplings are then matched to those of the full theory by calculations of particular observables [8, 9]. While a successful description of the phase transition for $SU(2)$ can be achieved in this way [10] (see also [11]), in the case of $SU(3)$ there remain so far several open couplings that cannot be matched easily.

In this paper, we study the possibility of reducing the full theory to an effective theory by using strong coupling expansions on a lattice. Such an approach was conjectured to be sensible in [12] and has been explored earlier in the literature [13–18]. It results in a three-dimensional effective theory of Polyakov loops. A common simplification was the neglect of spatial plaquettes, which has been argued not to influence the universal behaviour of the theory. Work where authors went beyond the spatial strong coupling limit is [19], see also [20] for recent developments on Polyakov loop extended strong coupling lattice QCD with staggered fermions.

Here we significantly extend this approach and calculate longer strong coupling series for the effective couplings, which are thus valid beyond the spatial strong coupling limit. Strong coupling series have a finite radius of convergence, which in this case is given by the deconfinement transition. Hence, our effective theory is valid in the confined phase and complementary to weak coupling approaches. We also investigate the influence of next-to-nearest neighbour Polyakov loop interaction terms which arise in higher orders. For our first studies we consider the pure gauge theories $SU(2)$ and $SU(3)$. After derivation of the effective theories of complex scalar fields in 3d, corresponding to the traces of the Polyakov loop and its hermitian conjugate, we study them by means of Monte Carlo simulations. In particular we determine the order and the critical couplings of the deconfinement phase transition and relate them to those of the original theories. We find qualitative and quantitative agreement with less than 6% deviations for the $\beta_c(N_\tau)$ up to $N_\tau = 16$, suggesting that these models are useful for the study of continuum physics.

The paper is structured as follows: in section 2 the effective actions for the two gauge groups are derived, with detailed discussion about the higher-order contributions to the effective couplings; then, in section 3, we present the Monte Carlo implementation of the effective models together with numerical results; section 4 provides the corresponding predictions for the original 4d theories and in section 5 we conclude.

2 Derivation of the effective theory

2.1 General strategy and $SU(2)$

Consider the partition function of a $(3+1)$ -dimensional lattice gauge field theory at finite temperature $(T = \frac{1}{aN_\tau})$ with gauge group $SU(N)$ and Wilson’s gauge action

$$Z = \int [dU_0] [dU_i] \exp \left[\frac{\beta}{2N} \sum_p \left(\text{tr } U_p + \text{tr } U_p^\dagger \right) \right], \quad \beta = \frac{2N}{g^2}. \quad (2.1)$$

Finite temperature and the bosonic nature of the degrees of freedom imply the use of periodic boundary conditions in the time direction.

In order to arrive at an effective three-dimensional theory, we integrate out the spatial degrees of freedom and get schematically [16]:

$$\begin{aligned} Z &= \int [dU_0] \exp [-S_{\text{eff}}] ; \\ -S_{\text{eff}} &= \ln \int [dU_i] \exp \left[\frac{\beta}{2N} \sum_p \left(\text{tr } U_p + \text{tr } U_p^\dagger \right) \right] \equiv \\ &\equiv \lambda_1 S_1 + \lambda_2 S_2 + \dots \end{aligned} \quad (2.2)$$

We expand around $\beta = 0$ and arrange the effective couplings $\lambda_n = \lambda_n(\beta, N_\tau)$ in increasing order in β of their leading terms. Thus, the λ_n become less important the higher n . As we shall see, the interaction terms S_n depend only on Polyakov loops

$$L_j \equiv \text{tr } W_j \equiv \text{tr } \prod_{\tau=1}^{N_\tau} U_0(\vec{x}_j, \tau) . \quad (2.3)$$

This is the reason for a “dimensional reduction” occurring here, as the time dimension is now implicit in the variables of the effective theory, which are fields defined on the spatial lattice. With sufficiently accurate knowledge of the relations $\lambda_n(\beta, N_\tau)$, we are able to convert the couplings of the three-dimensional theory to those of the full theory. In this work we are mainly interested in the deconfinement transition. Determining the critical parameters $\lambda_{n,c}$ of the effective theory then gives a whole array of critical $\beta_c(N_\tau)$ for - in principle - all N_τ . In the following we calculate strong coupling, i.e. small β , expansions of the leading λ_n .

Since the calculations are quite similar for different numbers of colours, we now specialise our derivation to the simpler case of $SU(2)$ and later provide the necessary changes for $SU(3)$. Using the character expansion as described e.g. in [21, 22], the effective action according to Eq. (2.2) can be written as

$$-S_{\text{eff}} = \ln \int [dU_i] \prod_p \left[1 + \sum_{r \neq 0} d_r a_r(\beta) \chi_r(U_p) \right] , \quad (2.4)$$

where the sum extends over all irreducible representations r with dimension d_r and character χ_r . The expansion coefficients $a_r(\beta)$ are accurately known [21] and in the following we use $u \equiv a_f$ as expansion parameter instead of β for its better apparent convergence. The logarithm in this definition allows us to use the method of moments and cumulants [23], and we get the following cluster expansion

$$\begin{aligned} -S_{\text{eff}} &= \sum_{C=(X_l^{n_l})} a(C) \prod_l \Phi(X_l; \{W_j\})^{n_l} ; \\ \Phi(X_l; \{W_j\}) &= \int [dU_i] \prod_{p \in X_l} d_{r_p} a_{r_p} \chi_{r_p}(U_p) , \end{aligned} \quad (2.5)$$

where the combinatorial factor $a(C)$ equals 1 for a single polymer X_i and -1 for two non-identical connected polymers. For clusters consisting of more than two polymers, $a(C)$

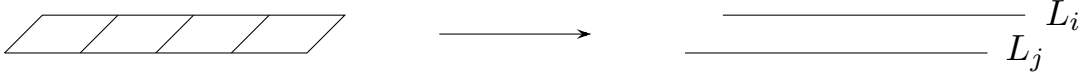


Figure 1. First graph with a nontrivial contribution after spatial integration for a lattice with temporal extent $N_\tau = 4$. Four plaquettes in the fundamental representation lead to an interaction term involving two adjacent fundamental Polyakov loops L_i and L_j .

depends on how these polymers are connected. In contrast to earlier calculations [24, 25], where also the temporal links were integrated over, the contribution Φ still depends on Wilson line variables W_j , which results in the interaction terms for the effective action, Eq. (2.2). Our task is then to group together all graphs yielding the same interaction terms up to some order in β , and this finally gives the strong coupling expansion of the corresponding effective coupling λ_n .

2.2 The spatial strong coupling limit

In earlier strong coupling calculations at finite temperature it has been customary to neglect spatial plaquettes. Let us briefly discuss this limit as it gives some important insights for the following. Neglecting spatial plaquettes, the integrations in Eq. (2.4) can be done applying the group integration rules

$$\int dU \chi_r(XU) \chi_s(U^{-1}Y) = \frac{\delta_{rs}}{d_r} \chi_r(XY) \quad (2.6)$$

$$\longrightarrow \int dU \chi_r(U) = \delta_{r,0} \quad (2.7)$$

on each spatial link and we get the partition function [14]:

$$Z = \int [dW] \prod_{\langle ij \rangle} \left[1 + \sum_{r \neq 0} \left[a_r(\beta) \right]^{N_\tau} \chi_r(W_i) \chi_r(W_j) \right], \quad (2.8)$$

where we replaced the integration over all temporal links with an integration over the Wilson line variables W_i as in [26]. This is justified since the integrand depends on temporal link variables only through the W_i .

Some important observations in this limit are:

- The summation extends only over pairs of nearest neighbours $\langle ij \rangle$, i.e. next-to-nearest neighbour interactions vanish without the inclusion of spatial plaquettes.
- Contributions from higher representations start with higher powers of β .
- The exponential function has cancelled, hence if we insist on having a partition function of the form $Z = \int \exp[-S]$, we have to introduce a logarithm in the action.

2.3 Leading order effective action

The leading order result of the effective action has first been calculated in [13] and corresponds to a sequence of N_τ plaquettes that wind around the lattice in temporal direction, cf. figure 1. Its contribution is given by:

$$\lambda_1 S_1 = u^{N_\tau} \sum_{\langle ij \rangle} L_i L_j. \quad (2.9)$$

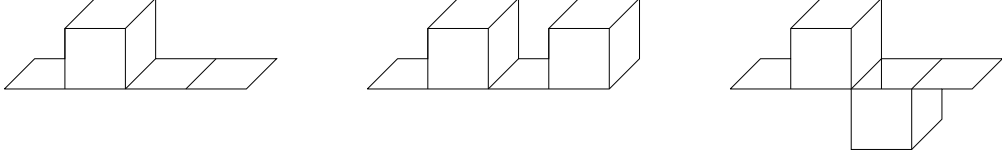


Figure 2. Left: First correction to the leading order graph, proportional to N_τ . Middle, right: Repetitions of this decoration.

Hence, to leading order the first coupling of the effective theory is $\lambda_1(u, N_\tau) = u^{N_\tau}$.

For additional terms of the series for λ_1 , we can use most of the graphs that also appear in the strong coupling expansion of the Polyakov loop susceptibility [25]. These corrections involve additional plaquettes, are hence of higher order in u and we call these attached plaquettes decorations. Let us note that repetitions of lower order decorations attached to planar graphs exponentiate and we can write

$$\lambda_1(u, N_\tau) = u^{N_\tau} \exp \left[N_\tau P(u, N_\tau) \right], \quad (2.10)$$

with some polynomial $P(u, N_\tau)$. This can be seen e.g. from the graphs shown in figure 2 and their corresponding contributions:

$$\begin{aligned} \text{Left:} \quad \Phi_1 &= u^{N_\tau} \left[4N_\tau u^4 \right] S_1; \\ \text{Middle:} \quad \Phi_2 &= u^{N_\tau} \left[\frac{1}{2!} (4N_\tau u^4) \cdot 4(N_\tau - 3)u^4 \right] S_1; \\ \text{Right:} \quad \Phi_3 &= u^{N_\tau} \left[4N_\tau u^4 \cdot 3N_\tau u^4 \right] S_1. \end{aligned} \quad (2.11)$$

Combining the three parts, we can write this, up to higher orders, as

$$\Phi_1 + \Phi_2 + \Phi_3 = u^{N_\tau} \exp \left[N_\tau (4u^4 - 12u^8) \right] S_1. \quad (2.12)$$

Of course, the polynomial in the exponential is only part of the complete result for λ_1 to that order. For example, there are other graphs contributing to order u^6 which are still missing in this correction. Nevertheless, in this exponentiated form the effective coupling corresponds to a partial resummation of higher order terms which may be expected to improve convergence behaviour. Let us remark that such an exponentiation has been observed also for the strong coupling expansion of the string tension.

Carrying out the calculations, we get the following results through order u^{10} in the corrections relative to the leading order graph:

$$\begin{aligned} \lambda_1(u, 2) &= u^2 \exp \left[2 \left(4u^4 - 8u^6 + \frac{134}{3}u^8 - \frac{49044}{405}u^{10} \right) \right], \\ \lambda_1(u, 3) &= u^3 \exp \left[3 \left(4u^4 - 4u^6 + \frac{128}{3}u^8 - \frac{36044}{405}u^{10} \right) \right], \\ \lambda_1(u, 4) &= u^4 \exp \left[4 \left(4u^4 - 4u^6 + \frac{140}{3}u^8 - \frac{37664}{405}u^{10} \right) \right], \\ \lambda_1(u, N_\tau \geq 5) &= u^{N_\tau} \exp \left[N_\tau \left(4u^4 - 4u^6 + \frac{140}{3}u^8 - \frac{36044}{405}u^{10} \right) \right]. \end{aligned} \quad (2.13)$$

For smaller N_τ some graphs do not contribute since the temporal extent of their decoration is $\geq N_\tau$ so that they do not fit into the lattice. The coefficients of the order n in the

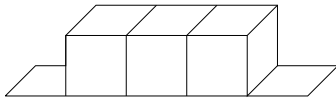


Figure 3. Shape of the most elongated graph contributing to λ_1 at order $n = 2(q+1)$, here in the case $q = 3$: only systems with $N_\tau > q$ can actually accommodate for it.

exponents of the effective couplings, Eq. (2.13), reach their $N_\tau = \infty$ values as soon as $N_\tau = n/2$. This can be understood as follows. Among all graphs contributing to the coefficient at order u^n , the most elongated in the time direction is of the type depicted in figure 3, with q consecutive lifted plaquettes, which brings in $n = 2(q+1)$ additional powers of u . Such a graph is included only if $N_\tau \geq q+1$ (in the moment-cumulant formalism a given polymer cannot occupy twice the same plaquette).

2.4 Higher order terms

There occur several types of higher order graphs: larger numbers of loops involved, Polyakov loops at distances larger than one and Polyakov loops in higher dimensional representations.

We begin by considering powers of the leading order term. Inspection of higher order terms shows that one can arrange a subclass of these terms in the following manner

$$\sum_{\langle ij \rangle} \left(\lambda_1 L_i L_j - \frac{\lambda_1^2}{2} L_i^2 L_j^2 + \frac{\lambda_1^3}{3} L_i^3 L_j^3 - \dots \right) = \sum_{\langle ij \rangle} \ln(1 + \lambda_1 L_i L_j) . \quad (2.14)$$

Thus, there are graphs that reproduce the emergence of the logarithm just as in the spatial strong coupling result, Eq. (2.8). In contrast to that case we have now the full effective coupling $\lambda_1(u, N_\tau)$ appearing in the logarithm instead of only its leading order term u^{N_τ} , which results if we restrict Eq. (2.8) to the fundamental representation. To see this, one calculates the corresponding graphs with $L_i^2 L_j^2$ or $L_i^3 L_j^3$, and the combinatorial factor $a(C)$ of Eq. (2.6) gives the correct prefactors for the series to represent a logarithm.

Next, let us consider couplings pertaining to next-to-nearest neighbour interactions. These appear once additional plaquettes are taken into account. Naively, the leading contribution should correspond to a planar graph with Polyakov loops at distance two. However, this graph is precisely cancelled by the contribution of the nearest-neighbour graph squared and its associated combinatorial factor -1 (figure 4). The leading non-zero contribution therefore comes from L-shaped graphs and is given by

$$\lambda_2(u, N_\tau) S_2 = N_\tau(N_\tau - 1) u^{2N_\tau+2} \sum_{[kl]} L_k L_l , \quad (2.15)$$

where we have two additional spatial plaquettes (figure 5) and we sum over all pairs of loops with a diagonal distance of $\sqrt{2}a$, abbreviated by $[kl]$. With the same steps leading to Eq. (2.14), we finally arrive at the $SU(2)$ partition function

$$Z = \int [dW] \prod_{\langle ij \rangle} [1 + \lambda_1 L_i L_j] \prod_{[kl]} [1 + \lambda_2 L_k L_l] . \quad (2.16)$$



Figure 4. Two graphs without spatial plaquettes that cancel against each other due to different signs.

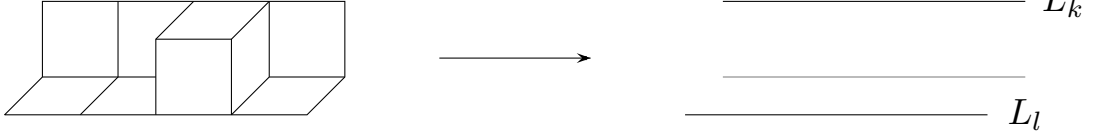


Figure 5. Leading order graph contributing to the interaction between loops at a distance $\sqrt{2}a$, denoted with $[kl]$ in the summations.

Let us further point out that corrections to the planar next-to-nearest neighbours, having a distance of $2a$, give to leading order

$$\lambda_3(u, N_\tau) S_3 \sim u^{2N_\tau+6} \sum_{\langle\langle mn \rangle\rangle} L_m L_n , \quad (2.17)$$

with an obvious notation for straight line next-to-nearest neighbours. The leading order graph is given in figure 6. Since these corrections are of higher order in u than the ones with distance $\sqrt{2}a$, we will omit them in this work. As we shall see later, the effective theory in case of $SU(2)$ works quite well even without next-to-nearest neighbours, hence we will quote explicit results for the coupling λ_2 for the case of $SU(3)$ only.

Finally, we include some remarks about the Polyakov loops in higher dimensional representations. Consider, e.g., the adjoint Polyakov loop: the leading order term emerging from a strong coupling expansion is

$$\lambda_a S_a = v^{N_\tau} \sum_{\langle ij \rangle} \chi_a(W_i) \chi_a(W_j) , \quad v = \frac{2}{3}u^2 + \frac{2}{9}u^4 + \frac{16}{135}u^6 + \dots$$

and hence $\lambda_a \sim u^{2N_\tau}$, which is formally of lower order than the coupling λ_2 . To next-to-leading order (valid for all $N_\tau \geq 2$) we have

$$\lambda_a = v^{N_\tau} \left(1 + N_\tau \frac{8}{3} \frac{u^6}{v} + \dots \right) . \quad (2.18)$$

Effects of higher representations have also been investigated in the literature [17, 18, 27].

2.5 The effective action for $SU(3)$

In the case of $SU(3)$ the same steps as for $SU(2)$ apply. The only difference we have to keep in mind is that $SU(3)$ also has an anti-fundamental representation and consequently there is also a complex conjugate Polyakov loop variable L_i^* . Thus we get the one-coupling and two-coupling partition functions

$$Z_1 = \int [dW] \prod_{\langle ij \rangle} [1 + \lambda_1 (L_i L_j^* + L_i^* L_j)] , \quad (2.19)$$

$$Z_2 = \int [dW] \prod_{\langle ij \rangle} [1 + \lambda_1 (L_i L_j^* + L_i^* L_j)] \prod_{[kl]} [1 + \lambda_2 (L_k L_l^* + L_k^* L_l)] . \quad (2.20)$$

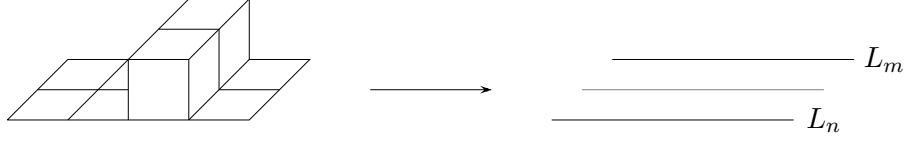


Figure 6. Leading order graph of next-to-nearest neighbours with distance $2a$.

The effective coupling $\lambda_1(u, N_\tau)$ is obtained as (for this gauge group, in view of the comparison that will be made with available 4d Yang-Mills simulation data, we consider only even values of N_τ ; however, analogous formulae hold for odd N_τ):

$$\begin{aligned}
\lambda_1(2, u) &= u^2 \exp \left[2 \left(4u^4 + 12u^5 - 18u^6 - 36u^7 \right. \right. \\
&\quad \left. \left. + \frac{219}{2}u^8 + \frac{1791}{10}u^9 + \frac{830517}{5120}u^{10} \right) \right] , \\
\lambda_1(4, u) &= u^4 \exp \left[4 \left(4u^4 + 12u^5 - 14u^6 - 36u^7 \right. \right. \\
&\quad \left. \left. + \frac{295}{2}u^8 + \frac{1851}{10}u^9 + \frac{1035317}{5120}u^{10} \right) \right] , \\
\lambda_1(N_\tau \geq 6, u) &= u^{N_\tau} \exp \left[N_\tau \left(4u^4 + 12u^5 - 14u^6 - 36u^7 \right. \right. \\
&\quad \left. \left. + \frac{295}{2}u^8 + \frac{1851}{10}u^9 + \frac{1055797}{5120}u^{10} \right) \right] . \quad (2.21)
\end{aligned}$$

For the first terms of the next-to-nearest neighbour coupling $\lambda_2(N_\tau, u)$ we find

$$\begin{aligned}
\lambda_2(2, u) &= u^4 \left[2u^2 + 6u^4 + 31u^6 \right] , \\
\lambda_2(4, u) &= u^8 \left[12u^2 + 26u^4 + 364u^6 \right] , \\
\lambda_2(6, u) &= u^{12} \left[30u^2 + 66u^4 \right] , \\
\lambda_2(N_\tau \geq 8, u) &= u^{2N_\tau} \left[N_\tau(N_\tau - 1)u^2 \right] , \quad (2.22)
\end{aligned}$$

while the leading coupling of adjoint loops is (valid for $N_\tau \geq 2$)

$$\lambda_a = v^{N_\tau} \left(1 + N_\tau \frac{3}{2} \frac{u^6}{v} + \dots \right), \quad v = \frac{9}{8}u^2 - \frac{9}{8}u^3 + \frac{81}{32}u^4 + \dots \quad (2.23)$$

3 Numerical simulation of the effective theories

In this section we proceed to evaluate the effective theories by Monte Carlo methods. After introducing a suitable algorithm, we discuss the strategy employed to extract critical couplings and the properties of phase transitions, and present detailed numerical results.

3.1 The one coupling model

For the purpose of numerical simulations, a further simplification is achieved by using the trace of the Polyakov loops for the path integral measure as degrees of freedom (complex numbers instead of matrices), and rewrite the one-coupling partition function for $SU(3)$, Eq. (2.19),

$$Z = \left(\prod_x \int dL_x \right) e^{-S_{\text{eff}}} ; \quad S_{\text{eff}} = - \sum_{\langle ij \rangle} \log(1 + 2\lambda_1 \text{Re} L_i L_j^*) - \sum_x V_x . \quad (3.1)$$

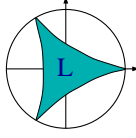


Figure 7. Domain for the complex numbers L_x in the $SU(3)$ effective theory.

The complex numbers L_x represent traces of $SU(3)$ matrices, and thus $|L_x| \leq 3$. The complex domain of L_x is thus the “three-pointed star” with radius 3, figure 7.

The potential term in S_{eff} is the Jacobian induced by the Haar measure of the original group integration and its actual form depends on the chosen parametrisation for L_x . Following [28], we write the trace of a $SU(3)$ matrix by rotating it to its diagonal form,

$$L_x(\theta, \phi) = e^{i\theta} + e^{i\phi} + e^{-i(\theta+\phi)}, \quad -\pi \leq \theta, \phi \leq +\pi. \quad (3.2)$$

In this case the potential is

$$V_x = \frac{1}{2} \log(27 - 18|L_x|^2 + 8\text{Re}L_x^3 - |L_x|^4). \quad (3.3)$$

The integration measure actually used in our simulation then takes the form

$$\int dL_x e^{V_x} = \int_{-\pi}^{+\pi} d\phi_x \int_{-\pi}^{+\pi} d\theta_x e^{V_x}. \quad (3.4)$$

When working on the $SU(2)$ theory, $-2 \leq L_x \leq +2$ is a real number and we simply have

$$\int_{-2}^{+2} dL_x e^{V_x}, \quad V_x = \frac{1}{2} \log(4 - L_x^2). \quad (3.5)$$

3.2 A “sign problem” and its solution

The effective theory described so far has lower dimensionality and simpler degrees of freedom per site than the initial Wilson action, suggesting a straightforward local Metropolis update based on accept/reject steps. This ideal situation is somewhat complicated by some sort of a “sign problem”.

Consider the effective partition function in Eq. (2.19). For couplings larger than some threshold, $\lambda > \lambda^T$, there are gauge configurations yielding negative contributions to Z , or, equivalently, for which the logarithms appearing in the effective action have negative arguments. Although Z remains overall positive, the Metropolis update ceases working when approaching this threshold value of the coupling.

For the $SU(3)$ action $\text{Re}L_i L_j^*$ can go down to $-9/2$ and the threshold coupling is $\lambda^T = 1/9$, while for $SU(2)$ we have $\lambda^T = 1/4$. In this work our interest is in the phase transition, and we shall see that for $SU(3)$ the critical coupling $\lambda_{1,c}$ happens to be close to λ^T . This sign problem is then a practical concern and a solution is called for. Fortunately, in the case of $SU(2)$ we have $\lambda_{1,c} \sim 0.2 < \lambda^T = 1/4$ and this problem can be ignored. We exploit this fact to test our workaround for the problem against the full solution.

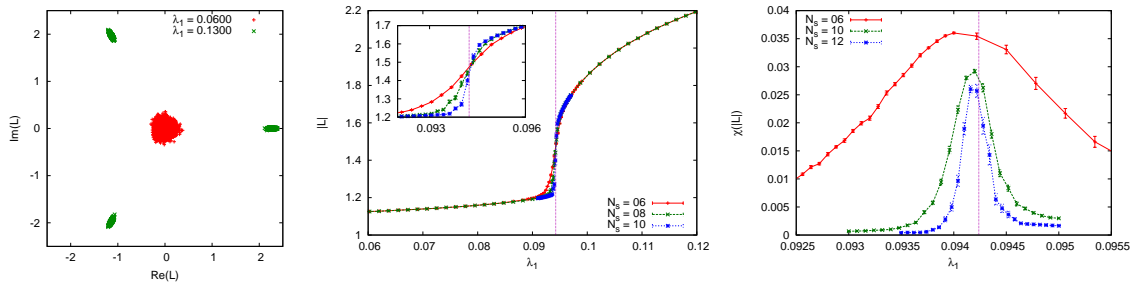


Figure 8. Left: Distribution of L for small and large λ_1 on a lattice with $N_s = 6$ and $M = 1$. Middle, Right: Expectation value of $|L|$ and its susceptibility. The vertical line marks the infinite-volume transition.

Our approach to overcome this problem is the following: we Taylor-expand the logarithm in the effective action to some order M in powers of $q \equiv \lambda_1 \text{Re} L_i L_j^*$, which effectively undoes the resummation as in Eq. (2.14),

$$S_{\text{eff}}^{(M)} = - \sum_x V_x - \sum_{\langle ij \rangle} \left(2q - 2q^2 + \frac{8}{3}q^3 - 4q^4 + \frac{32}{5}q^5 - \dots - (-1)^M \frac{2^M}{M} q^M \right). \quad (3.6)$$

We thus obtain a family of models which are, by construction, free of the mentioned problem, and are expected to converge to the full theory as $M \rightarrow \infty$. The strategy is then to find the series of critical points $\lambda_{1,c}(M)$ and to look for their convergence behaviour as M increases.

In order to have a critical model, moreover, one must truncate the expansion at an odd power M : for even truncations, indeed, the slope of the effective action as a function of q , corresponding to a force, vanishes for $2q \lesssim 1$, and never triggers a symmetry breaking by favouring aligned neighbours. Let us observe, incidentally, that this limitation is absent in the $SU(2)$ case, exactly because the transition region is far from the threshold coupling and the value of $\lambda_1 L_i L_j$ is always too far from 1 for this phenomenon to take place.

3.3 Phase structure, critical coupling and finite size analysis

Our first task is to establish the phase structure of the effective theory, where we focus on the physically interesting case of $SU(3)$. Based on the global $Z(3)$ symmetry of the model, one expects spontaneous breaking of that symmetry for some critical value of the coupling $\lambda_{1,c}$. Figure 8 shows the behaviour of the field variable L as a function of λ_1 . As expected from the 4d parent theory, there is indeed a transition from a disordered or mixed phase, with values of L scattering about zero, to an ordered phase at large coupling where the three $Z(3)$ -phases are populated separately. In the thermodynamic limit, one of these vacua will be chosen and the symmetry is broken spontaneously, $\langle L \rangle = 0$ for $\lambda_1 < \lambda_{1,c}$ and $\langle L \rangle \neq 0$ for $\lambda_1 > \lambda_{1,c}$. Correspondingly, the expectation value of $|L|$ rises abruptly at some critical coupling $\lambda_{1,c}$, as shown in figure 8 (middle). On a finite size lattice, the phase transition is smoothed out, non-analyticities are approached gradually with growing volume, as the figure illustrates.

The general technique to locate the infinite-volume critical coupling, $\lambda_{1,c}$, is based on a finite-size scaling analysis. A variety of cubic systems are simulated and for each one a pseudo-critical point $\lambda_{1,c}(N_s)$ is found. As a function of lattice side length N_s , close enough to the thermodynamic limit these scale as

$$\lambda_{1,c}(N_s) = \lambda_{1,c} + bN_s^{-1/\nu} . \quad (3.7)$$

The relevant universal values for the critical index are $\nu = 0.63002$ for 3d Ising [29] and $\nu = 1/3$ for a first order transition. In practice we found it sufficient to use spatial volumes $N_s = 6, \dots, 12$ in order to extrapolate to the thermodynamic limit. In this way, the whole data production can be carried out in a handful of days on a modest desktop PC.

The pseudo-critical coupling can be defined in a variety of ways: one possibility is to employ the energy observable:

$$E = -\frac{1}{\lambda_1} S'_{\text{eff}} , \quad (3.8)$$

where the prime denotes omission of the potential term V_x . For the $M = 1$ model, this coincides with the usual energy,¹ while at higher truncations (as well as in the non-truncated formulation) S_{eff} is non-linear in the coupling. For this reason, the energy is used only in the $M = 1$ particular case. Other natural observables are based on the modulus of the Polyakov loop, $|L|$. We consider the Binder cumulant

$$B(|L|) = 1 - \frac{\langle |L|^4 \rangle}{3\langle |L|^2 \rangle^2} , \quad (3.9)$$

whose minimum defines a pseudo-critical coupling, and the susceptibility

$$\chi(|L|) = \left\langle \left(|L| - \langle |L| \rangle \right)^2 \right\rangle , \quad (3.10)$$

whose maximum is taken as pseudo-critical coupling, cf. figure 8 (right). Having various definitions of pseudo-critical couplings, one can check for the mutual consistency of the infinite-volume critical points coming from them.

3.4 Critical coupling and order of the transition for $SU(3)$

The truncated theories with $M = 1, 3, 5$ were simulated on lattices with spatial sizes $N_s = 6, 8, 10$ (plus $N_s = 12$ for the $M = 1$ theory). For each volume, ~ 30 values of the couplings are sampled by $\sim 10^6$ update sweeps each. Measurements were taken every ~ 30 updates.

We begin our presentation of results with the $SU(3)$ family of effective theories, where we find a first-order transition regardless of the particular truncation employed. A practical difficulty is the related occurrence of metastabilities with extremely long thermalisation times $\propto \exp(cN_s^3)$. The local Metropolis update requires a number of iterations akin to a tunnelling time in order to dispel configurations with two halves of the system associated with different vacua. To take care of this problem, very long trajectories are inspected by cutting out an initial block of configurations until stability is found in the resulting

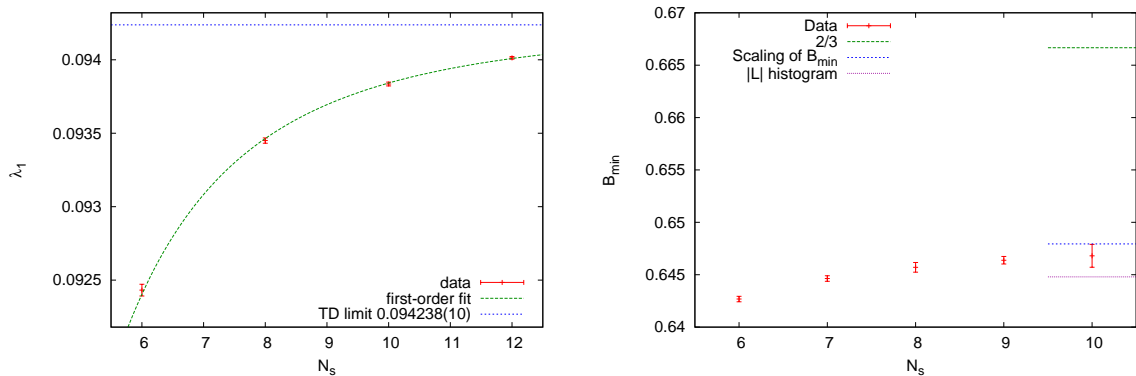


Figure 9. Left: Position of the minimum of the Binder cumulant $B(E)$ for $SU(3)$, $M = 1$, for different lattice sizes. The horizontal line is the thermodynamic limit resulting from the fit to Eq. (3.7). Right: Behaviour of $B_{\min}(N_s)$, along with its thermodynamic limit obtained with the $\mathcal{O}(N_s^{-3})$ scaling law and the independent estimate B_∞ from the $|L|$ histogram. Also the second-order limit value $2/3$ is shown.

averages: for instance, a system with size $N_s = 16$ would require, around criticality, $\sim 10^6$ update sweeps to thermalise.

First we consider the model with $M = 1$. The first-order nature of the transition is established by fitting the pseudo-critical couplings to the scaling law, Eq. (3.7), with $\nu = 1/3$, as shown in figure 9 (left). The same conclusion is reached when analysing the scaling of the minimum $B_{\min}(N_s)$ of $B(|L|)$, figure 9 (right): this quantity, in the $N_s \rightarrow \infty$ limit, approaches the saturation value $2/3$ if and only if the transition is second-order, while in case of a first-order point the thermodynamic limit is given by [30]:

$$B_\infty = \frac{2}{3} - \frac{1}{12} \left(\frac{|L|_1}{|L|_2} - \frac{|L|_2}{|L|_1} \right)^2, \quad (3.11)$$

where $|L|_1$ and $|L|_2$ are the local maxima of the $|L|$ double-peaked histogram. Inspection of the $|L|$ distribution shows indeed a two-peaked shape (figure 10) that becomes narrower and higher at increasing system volumes. It is then possible to give an independent estimate for B_∞ and compare it with that from the scaling of the $B(|L|)$ minimum. The comparison (figure 9, right) confirms indeed the first-order nature of the transition, while some slight mismatch (less than two standard deviations) remains between the two estimates. This is most likely due to the presence of subleading terms in the scaling of B_{\min} . As demonstrated in [31], the scaling law to NLO has the form

$$B_{\min}(N_s) = B_\infty + B^{(2)} N_s^{-3} + B^{(3)} N_s^{-6}, \quad (3.12)$$

and it is necessary to explore very large lattices to observe the leading-order scaling.

¹Also in the $\lambda \rightarrow 0$ limit, at any truncation, this definition recovers the standard energy term.

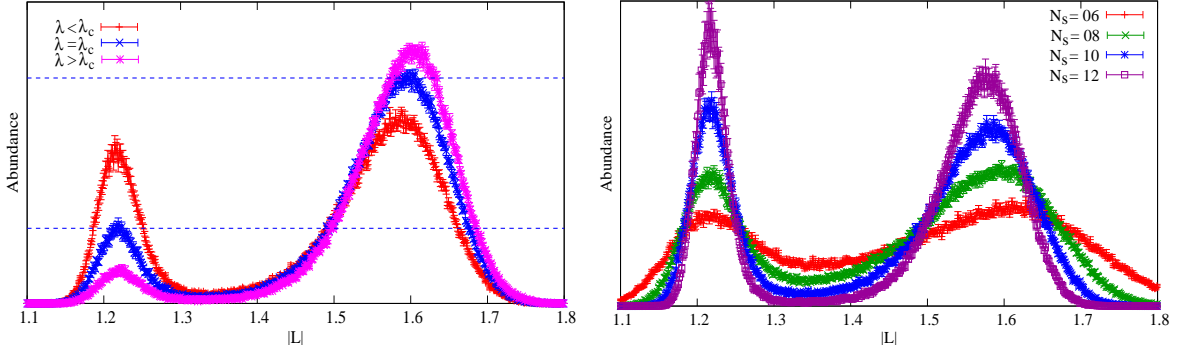


Figure 10. Left: Histogram for $|L|$ of the $SU(3)$ theory on $N_s = 10$ with $M = 1$. The three curves have been measured with λ_1 slightly below, exactly at and slightly above pseudo-criticality. The horizontal lines are guides to the eye and mark the peak on the right as being, for the pseudo-critical curve, exactly three times as high as the one on the left. Right: Histogram of the $SU(3)$ $|L|$ for four different system sizes N_s at the true critical point. The size-dependence of the peaks' position was taken into account in estimating B_∞ with Eq. (3.11).

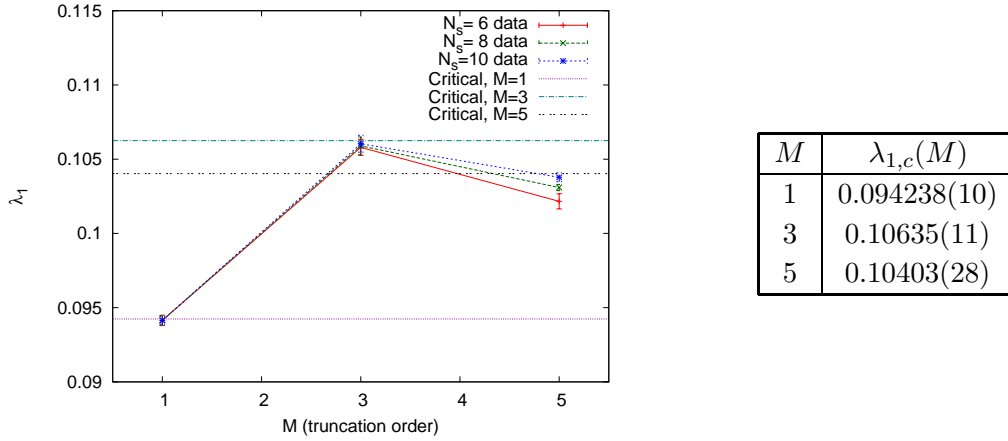


Figure 11. Critical points in the thermodynamical limit (horizontal lines) and pseudocritical values (data points) on three spatial sizes, for the $SU(3)$ one-coupling model truncated at $M = 1, 3, 5$.

In the next step we need to investigate the behaviour of the models with higher M . Again we observe first order transitions, which become sharper with increasing M . Moreover, finite-size effects are stronger for higher M , figure 11. The critical couplings identified for the $M = 1, 3, 5$ effective theories in the thermodynamic limit are also quoted in figure 11. Judging from these three values, the series seems to be rapidly converging, with only $\sim 3\%$ difference between $M = 3, 5$. The residual difference between this estimate and the $M = \infty$ critical coupling is completely subdominant compared to the other systematic errors contributing to the final results. Also, the direct comparison with the $SU(2)$ case below, where the $M = \infty$ data are directly available, supports a rapid convergence, figure 13.

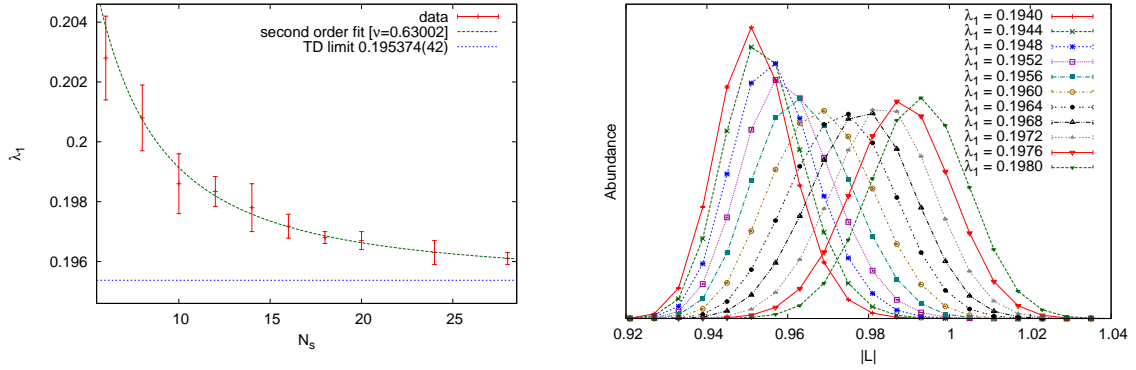


Figure 12. $SU(2)$ with $M = 1$; Left: Location of maximum of the E -susceptibility, fitted to the 3D Ising scaling law. Right: Histogram for $|L|$ at $N_s = 20$.

3.5 Critical coupling and order of the transition for $SU(2)$

In the case of the $SU(2)$ models, the same analysis was carried out. Since here we find second-order transitions, the metastability problems are absent and the thermalisation times are orders of magnitude shorter (e.g. around 4000 update sweeps at $N_s = 16$ around criticality). This enabled us to study larger system sizes up to $N_s = 28$ without much computational effort.

The same approaches as before clearly exhibit the second order nature of the transition, using the scaling law for the pseudo-critical points and the histogram for $|L|$ (see figure 12), as well as the corresponding Binder cumulant thermodynamic limit which in this case reaches smoothly the value $2/3$. Figure 12 shows the results for the $M = 1$ model. However, as indicated before, in the case of $SU(2)$ we can directly work with the full $M = \infty$ model and thus check for the systematic errors when a finite M truncation is used. This is shown in figure 13, explicitly we find

$$\lambda_{1,c}(M = 1) = 0.195374(42) \quad ; \quad \lambda_{1,c}(M = \infty) = 0.21423(70). \quad (3.13)$$

Indeed we observe rapid convergence on the $M = \infty$ results, in accord with our findings for $SU(3)$. We thus conclude that the truncation in M does not affect the results significantly and proves to be a viable way of dealing with the numerical difficulties discussed above.

3.6 Two-coupling models for $SU(3)$

In this section we study the influence of including a second coupling. We start with the leading next-to-nearest-neighbour interaction, specified by the model with a second coupling λ_2 , Eq. (2.16). For $SU(3)$, the two-coupling partition function reads

$$Z = \left(\prod_x \int dL_x \right) \prod_{\langle ij \rangle} (1 + 2\lambda_1 \text{Re} L_i L_j^*) \prod_{[kl]} (1 + 2\lambda_2 \text{Re} L_k L_l^*) e^{\sum_x V_x}. \quad (3.14)$$

As discussed previously, we neglect a third coupling related to next-to-nearest-neighbour interaction between loops at distance $2a$ since it starts at higher order than λ_2 .

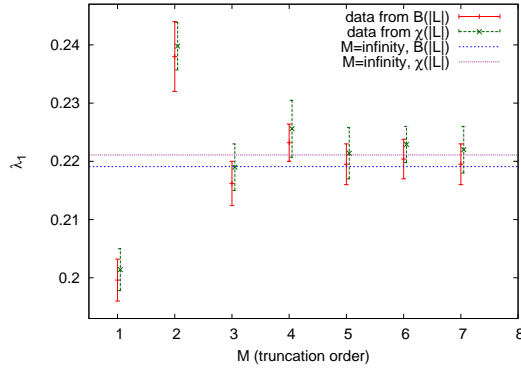


Figure 13. $\lambda_{1,c}(N_s = 8)$ for $SU(2)$ and various truncations. Estimates from $B(|L|), \chi(|L|)$ are shown; horizontal lines mark the values for the model without truncations ($M = \infty$).

In a natural extension of the critical point of the one-coupling model, there is now a critical line $\lambda_{1,c}(\lambda_2)$ separating the ordered from the disordered phase in the two-dimensional parameter space. However, not all points on this line are related to the physics of the 4d thermal theory. Once a particular N_τ is fixed, both λ_i depend on the expansion parameter $u(\beta)$ alone. Eliminating u , the curves $\lambda_1^{(N_\tau)}(\lambda_2)$ can be constructed, which represent the parameter space describing the physics of the 4d thermal model for a given N_τ . The critical couplings relevant for us are thus the intersections between the critical line of the effective two-coupling model and the curves specifying the map to a particular N_τ lattice.

We remark that the second factor in the partition function, Eq. (3.14), has the same kind of “sign problem” as the first one, calling for an analogous solution. Some attention needs to be paid to truncating the expansion of the two logarithms in a consistent way. We include all terms which contribute to the desired power of u from both expansions, for all values of N_τ . Based on our previous results, we want to keep terms up to $M = 3$ for the λ_1 part, and thus consider the leading second coupling term $M = 1$, which we denote with $(M_1, M_2) = (3, 1)$. Corrections by higher powers M_2 are formally of higher order in u , and we have checked numerically that their effect is completely negligible.

In order to locate the critical line $\lambda_{1,c}(\lambda_2)$, we fix 11 different values of λ_2 in the range $[0.002, 0.007]$ and scan in λ_1 in order to identify the pseudo-critical points, which can then be extrapolated to the thermodynamic limit. It turns out that, on a given volume, $\lambda_{1,c}(\lambda_2)$ is well described by a linear interpolation, cf. figure 14 (left). Moreover, the inclusion of the second coupling appears to diminish finite size effects. Since all three volumes shown in figure 14 (left) are consistent within errors, we quote the result from the largest lattice for the critical line,

$$\lambda_{1,c} = a + b\lambda_2 \quad \text{with} \quad a = 0.10628(8), \quad b = -1.891(4). \quad (3.15)$$

The value of a is consistent with the $M = 3$ critical point in the one-coupling theory.

Also shown in figure 14 (left) are the lines $\lambda_1^{(N_\tau)}(\lambda_2)$ for $N_\tau = 4, 6, 8$. One observes that they rapidly accumulate towards $\lambda_2 \simeq 0$. Only for the lowest values of N_τ , corresponding to coarse lattices in the 4d theory, does the adoption of the two-coupling model make

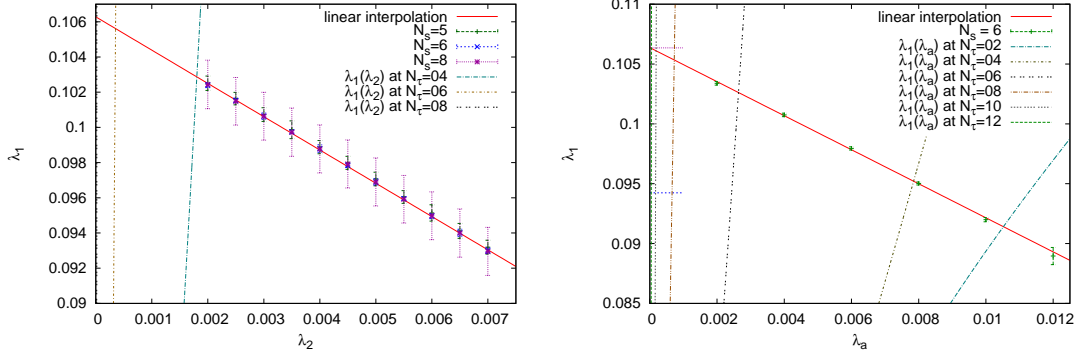


Figure 14. Critical line in the $SU(3)$ two-coupling space, determined from $\chi(|L|)$. Dashed lines give the parameter space representing a 4d theory with fixed N_τ . Left: (λ_1, λ_2) . Right: (λ_1, λ_a) .

any difference. For finer lattices, of interest for continuum physics, the results are within statistical errors indistinguishable from the simpler one-coupling theory.

Next, we are considering a two coupling theory with λ_1, λ_a . In this case the partition function reads

$$Z = \left(\prod_x \int dL_x \right) \prod_{\langle ij \rangle} (1 + 2\lambda_1 \text{Re} L_i L_j^*) \prod_{\langle ij \rangle} e^{\lambda_a (\text{Tr}^{(a)} W_i) (\text{Tr}^{(a)} W_j)} e^{\sum_x V_x}. \quad (3.16)$$

Here $\text{Tr}^{(a)}$ denotes the trace in the adjoint representation, $\text{Tr}^{(a)} W = |\text{Tr} W|^2 - 1$, which can be used to rewrite the action in terms of fundamental loops. For the numerical evaluation, we again expand the λ_1, λ_a terms to $(M_1 = 3, M_2 = 1)$, and proceed in complete analogy as in the case discussed above. The result for the critical line in this two-coupling space is shown in figure 14 (right). Here we find

$$\lambda_{1,c} = a + b\lambda_a \quad \text{with} \quad a = 0.10637(15), \quad b = -1.422(22). \quad (3.17)$$

Once more, the set of curves intersecting the critical line correspond to lines of fixed N_τ in the 4d theory. We observe that λ_a has slightly larger effect than λ_2 at fixed N_τ , in accord with the fact that it starts at lower order in u , cf. Eq. (2.23). Nevertheless, its influence is smaller than that of the strong coupling truncation in λ_1 , as we shall see, and hence negligible at this order.

4 Mapping back to 4d Yang-Mills

Having established the critical couplings for our effective theories and tested their reliability, we are now ready to map them back to the original thermal Yang-Mills theories by using Eqs. (2.13, 2.21). In Tables 1, 2 we collect the values for the critical gauge couplings, β_c , obtained in this way from the effective theories and compare them to the values obtained from simulations of the full 4d theories for $SU(2), SU(3)$, respectively.

The agreement is remarkable in all cases, with the relative error of the effective theory

N_τ	$M = 1$	$M = \infty$	4d YM
3	2.15537(89)	2.1929(13)	2.1768(30)
4	2.28700(55)	2.3102(08)	2.2991(02)
5	2.36758(40)	2.3847(06)	2.3726(45)
6	2.41629(32)	2.4297(05)	2.4265(30)
8	2.47419(22)	2.4836(03)	2.5104(02)
12	2.52821(14)	2.5341(02)	2.6355(10)
16	2.55390(10)	2.5582(02)	2.7310(20)

Table 1. Critical couplings β_c for $SU(2)$ from two effective theories compared to simulations of the 4d theory [32–34].

N_τ	$M = 1$	$M = 3$	$M_1, M_2(\lambda_2) = 3, 1$	$M_1, M_2(\lambda_a) = 3, 1$	4d YM
4	5.768	5.830	5.813	5.773	5.6925(002)
6	6.139	6.173	6.172	6.164	5.8941(005)
8	6.300	6.324	6.324	6.322	6.0010(250)
10	6.390	6.408	6.408	6.408	6.1600(070)
12	6.448	6.462	6.462	6.462	6.2680(120)
14	6.488	6.500	6.500	6.500	6.3830(100)
16	6.517	6.528	6.528	6.528	6.4500(500)

Table 2. Critical couplings β_c for $SU(3)$ from different effective theories compared to simulations of the 4d theory [33, 35].

results compared to the full ones shown in figure 15. The comparison of alternative truncations of the logarithm shows once more that it has almost no influence on the accuracy of the final result, as described earlier. Interestingly, there appears to be a ‘region of best agreement’, with the deviation growing both for small and large N_τ . We ascribe this to the fact that there are two competing systematic errors, as discussed earlier: the validity of the strong coupling series for a given coupling λ_i is better the smaller β and hence N_τ , whereas the truncation of the next-to-nearest neighbour interactions gains validity with growing N_τ . In particular in the case of $SU(3)$, there appears to be a cancellation of the two kinds of systematics, rendering the effective description better for the original theory on finer lattices.

In order to assess the systematics of the strong coupling series, figure 16 (left) shows the difference in β_c based on the one-coupling model when series of different depth are used for $\lambda_1(\beta)$. Satisfactory convergence behaviour is observed. For the case of $SU(2)$ a comparison with a non-perturbative derivation of the effective theory is possible. Figure 16 (right) compares $\lambda_{1,c}$ in terms of our strong coupling series with a determination by inverse Monte Carlo [17] (see [18] for $SU(3)$). Again, we observe good convergence of the strong coupling series to the full result. However, these plots also illustrate that the error due to truncation of the strong coupling series of the first coupling is larger than the neglect of

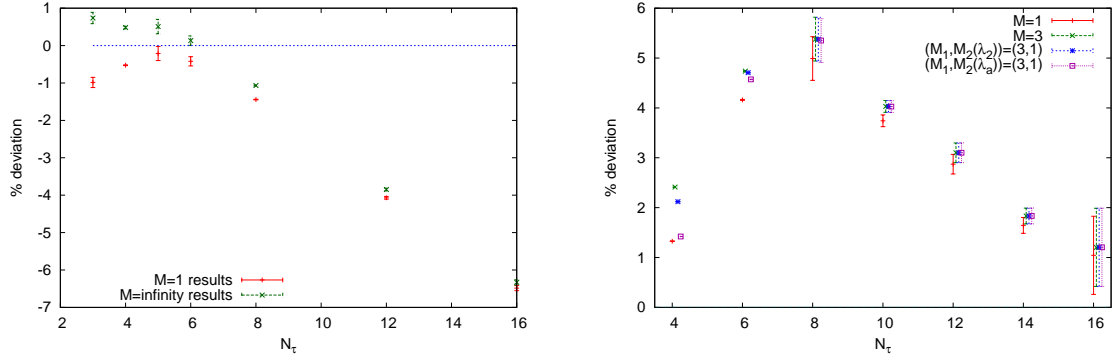


Figure 15. Relative error of β_c predicted by the effective theories when compared to simulations of the 4d theories, for $SU(2)$ (left) and $SU(3)$ (right).

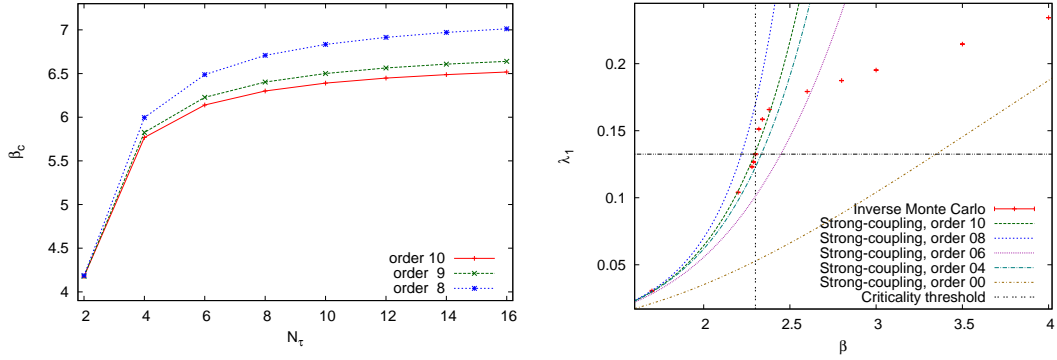


Figure 16. Left: β_c for $SU(3)$ from $\lambda_{1,c}(\beta)$ evaluated to 8th, 9th and 10th order, Eqs. (2.21). Right: $\lambda_1(\beta)$ for $SU(2)$ and $N_\tau = 4$ from strong-coupling expansion and inverse Monte Carlo [17].

higher couplings. We also attempted to improve the convergence of the series with Padé analysis, which however was not particularly successful, apart from confirming the order of magnitude of the estimated systematic uncertainties.

Figure 16 (right) illustrates the range of validity of the strong coupling derivation of the effective couplings. The non-perturbatively determined $\lambda_1(\beta)$ appears to change curvature at β_c , whereas the estimates based on the strong coupling series do not. This is consistent with β_c marking the radius of convergence also for the series expansion of the effective coupling λ_1 . Thus, the inverse Monte Carlo approach has a wider range of validity whereas the series approach furnishes analytically known mappings between the full and effective theories.

5 Conclusions

Employing strong coupling expansions, we have derived a dimensionally reduced, centre-symmetric effective description for lattice pure gauge theories at finite temperature. The effective theory is formulated in terms of scalar Polyakov loop variables and does not involve

any matrix degrees of freedom. Contrary to earlier derivations based on the lattice theory, we have included spatial plaquettes systematically. The effective theory has an infinite number of interaction terms with increasing degree of non-locality. Each of its couplings can be computed as a series in the original lattice gauge coupling β for any value of N_τ . We have explicitly calculated up to seven terms in the nearest-neighbour interaction and up to three terms in the next-to-nearest neighbour interactions. Furthermore, we have shown that other interaction terms are formally of higher order than the calculated ones. These calculations can be systematically improved in the future, if desired.

In the second part of the paper, we have performed detailed numerical studies of the effective theory for the cases of $SU(2)$ and $SU(3)$, focusing on the description of its order/disorder phase transition, which is related to the deconfinement transition of the 4d thermal theories. We computed the critical couplings and found the transition to correspond to 3d Ising for $SU(2)$ and first order for $SU(3)$. Explicit numerical checks with different approximations show that next-to-nearest neighbour couplings have negligible numerical effects, and furthermore demonstrate good convergence behaviour of the strong coupling series. Using the analytic expressions calculated earlier, the critical couplings can be converted to values for $\beta_c(N_\tau)$ predicting the deconfinement transition in the original 4d thermal theories. For lattices with $N_\tau = 4 - 16$, we found no more than 6% deviations from those calculated in simulations of the 4d theories.

In conclusion, we have given a successful description of the deconfinement transition of 4d $SU(N)$ Yang-Mills theories in terms of a dimensionally reduced $Z(N)$ -model derived by a strong coupling expansions. Future work might push for increased precision by inclusion of higher orders, which would entail more interaction terms and higher representation loops. Our model might also be of interest for numerical investigations of the deconfinement transition for $SU(N)$ with $N > 3$, cf. [36] and references therein. However, we believe at this stage it would be most interesting to extend this approach towards physical QCD by including fermions and finite baryon density, e.g. by means of a hopping parameter expansion [25, 37].

Acknowledgments

We thank Rob Pisarski for discussions and valuable comments on the manuscript. S. L. and O. P. are partially supported by the German BMBF grant *FAIR theory: the QCD phase diagram at vanishing and finite baryon density*, 06MS9150, and by the Helmholtz International Center for FAIR within the LOEWE program of the State of Hesse. J. L. acknowledges financial support by the EU project *Study of Strongly interacting Matter*, No. 227431, and by the BMBF under the project *Heavy Quarks as a Bridge between Heavy Ion Collisions and QCD*, 06BI9002.

References

- [1] A. D. Linde, *Infrared Problem In Thermodynamics Of The Yang-Mills Gas*, Phys. Lett. B **96** (1980) 289.

- [2] P. H. Ginsparg, *First Order And Second Order Phase Transitions In Gauge Theories At Finite Temperature*, Nucl. Phys. B **170** (1980) 388;
- [3] T. Appelquist and R. D. Pisarski, *High-Temperature Yang-Mills Theories And Three-Dimensional Quantum Chromodynamics*, Phys. Rev. D **23** (1981) 2305.
- [4] W. Buchmüller and O. Philipsen, *Phase structure and phase transition of the $SU(2)$ Higgs model in three-dimensions*, Nucl. Phys. B **443** (1995) 47 [arXiv:hep-ph/9411334].
- [5] K. Kajantie, M. Laine, K. Rummukainen and M. E. Shaposhnikov, *The Electroweak Phase Transition: A Non-Perturbative Analysis*, Nucl. Phys. B **466** (1996) 189 [arXiv:hep-lat/9510020].
- [6] F. Csikor, Z. Fodor and J. Heitger, *Endpoint of the hot electroweak phase transition*, Phys. Rev. Lett. **82** (1999) 21 [arXiv:hep-ph/9809291].
- [7] K. Kajantie, M. Laine, K. Rummukainen and M. E. Shaposhnikov, *3d $SU(N)$ + adjoint Higgs theory and finite-temperature QCD*, Nucl. Phys. B **503** (1997) 357 [arXiv:hep-ph/9704416].
- [8] A. Vuorinen and L. G. Yaffe, *$Z(3)$ -symmetric effective theory for $SU(3)$ Yang-Mills theory at high temperature*, Phys. Rev. D **74** (2006) 025011 [arXiv:hep-ph/0604100].
- [9] R. D. Pisarski, *Effective theory of Wilson lines and deconfinement*, Phys. Rev. D **74** (2006) 121703 [arXiv:hep-ph/0608242].
- [10] Ph. de Forcrand, A. Kurkela and A. Vuorinen, *Center-Symmetric Effective Theory for High-Temperature $SU(2)$ Yang-Mills Theory*, Phys. Rev. D **77** (2008) 125014 [arXiv:0801.1566 [hep-ph]].
- [11] A. Dumitru, D. Smith *Eigenvalue repulsion in an effective theory of $SU(2)$ Wilson lines in three dimensions*, Phys. Rev. D **77** (2008) 094022 [arXiv:0711.0868v1 [hep-lat]].
- [12] B. Svetitsky and L. G. Yaffe, *Critical Behavior At Finite Temperature Confinement Transitions*, Nucl. Phys. B **210** (1982) 423.
- [13] J. Polonyi and K. Szlachanyi, *Phase Transition From Strong Coupling Expansion*, Phys. Lett. B **110** (1982) 395.
- [14] F. Green and F. Karsch, *Mean Field Analysis Of $SU(N)$ Deconfining Transitions In The Presence Of Dynamical Quarks*, Nucl. Phys. B **238** (1984) 297.
- [15] A. Gocksch and M. Ogilvie, *Finite Temperature Deconfinement And Chiral Symmetry Restoration At Strong Coupling*, Phys. Rev. D **31** (1985) 877.
- [16] M. Gross and J. F. Wheeler, *On The Order Of The $SU(N)$ Deconfinement Phase Transition*, Nucl. Phys. B **240** (1984) 253.
- [17] T. Heinzl, T. Kaestner and A. Wipf, *Effective actions for the $SU(2)$ confinement-deconfinement phase transition*, Phys. Rev. D **72** (2005) 065005 [arXiv:hep-lat/0502013].
- [18] C. Wozar, T. Kaestner, A. Wipf and T. Heinzl, *Inverse Monte-Carlo determination of effective lattice models for $SU(3)$ Yang-Mills theory at finite temperature*, Phys. Rev. D **76** (2007) 085004 [arXiv:0704.2570 [hep-lat]].
- [19] M. Billò, M. Caselle, A. D’Adda and S. Panzeri, *Toward an analytic determination of the deconfinement temperature in $SU(2)$ L.G.T.*, Nucl. Phys. B **472** (1996) 163 [arXiv:hep-lat/9601020].

- [20] T. Z. Nakano, K. Miura and A. Ohnishi, *Chiral and deconfinement transitions in strong coupling lattice QCD with finite coupling and Polyakov loop effects*, arXiv:1009.1518 [hep-lat].
- [21] I. Montvay and G. Münster, *Quantum fields on a lattice*, Cambridge, UK: Univ. Pr. (1994) 491 p. (Cambridge monographs on mathematical physics).
- [22] J. M. Drouffe and J. B. Zuber, *Strong Coupling And Mean Field Methods In LDumitru2003:hpattice Gauge Theories*, Phys. Rept. **102**, 1 (1983).
- [23] G. Münster, *Vortex Free Energy And String Tension At Strong And Intermediate Coupling*, Phys. Lett. B **95** (1980) 59.
- [24] J. Langelage, G. Münster and O. Philipsen, *Strong coupling expansion for finite temperature Yang-Mills theory in the confined phase*, JHEP **0807** (2008) 036 [arXiv:0805.1163 [hep-lat]].
- [25] J. Langelage and O. Philipsen, *The deconfinement transition of finite density QCD with heavy quarks from strong coupling series*, JHEP **1001** (2010) 089 [arXiv:0911.2577 [hep-lat]].
- [26] M. Mathur, *Landau Ginzburg Model And Deconfinement Transition For Extended SU(2) Wilson Action*, arXiv:hep-lat/9501036.
- [27] A. Dumitru, Y. Hatta, J. Lenaghan, K. Orginos and R. D. Pisarski, *Deconfining phase transition as a matrix model of renormalized Polyakov loops*, Phys. Rev. D **70** (2004) 034511 [arXiv:hep-th/0311223].
- [28] M. Gross, J. Bartholomew and D. Hochberg, *SU(N) deconfinement transition and the N-state clock model*, Report No. EFI-83-35-CHICAGO, 1983.
- [29] M. Hasenbusch, *A Finite Size Scaling Study of Lattice Models in the 3D Ising Universality Class*, arXiv:1004.4486.
- [30] J. Lee and J. M. Kosterlitz, *Finite-size scaling and Monte Carlo simulations of first-order phase transitions*, Phys. Rev. B **43** (1991) 3265.
- [31] A. Billoire, T. Neuhaus and B. Berg, *Observation of FSS for a first-order phase transition*, Nucl. Phys. B **396** (1993) 779.
- [32] I. L. Bogolubsky, V. K. Mitrjushkin, A. V. Sergeev, M. Müller-Preussker and H. Stüben, *Polyakov loops and Binder cumulants in SU(2) theory on large lattices*, Nucl. Phys. Proc. Suppl. **129** (2004) 611.
- [33] J. Fingberg, U. M. Heller and F. Karsch, *Scaling and asymptotic scaling in the SU(2) gauge theory*, Nucl. Phys. B **392** (1993) 493.
- [34] A. Velytsky, *Finite temperature SU(2) gauge theory: critical coupling and universality class*, Int. J. Mod. Phys. C **19**, 1079 (2008) [arXiv:0711.0748 [hep-lat]].
- [35] J. Kogut, M. Stone and H. W. Wyld, *Deconfinement and Chiral Symmetry Restoration at Finite Temperatures in SU(2) and SU(3) Gauge Theories*, Phys. Rev. Lett. **50** (1983) 393.
- [36] M. Panero, *Thermodynamics of the QCD plasma and the large-N limit*, Phys. Rev. Lett. **103** (2009) 232001 [arXiv:0907.3719 [hep-lat]].
- [37] J. Langelage and O. Philipsen, *The pressure of strong coupling lattice QCD with heavy quarks, the hadron resonance gas model and the large N limit*, JHEP **1004** (2010) 055 [arXiv:1002.1507 [hep-lat]].